CDF/ANAL/TOP/CDFR/11053

v2

Search for W'-like resonances decaying to tb in the $\not\!\!E_T$ plus jets sample with the full CDF dataset

F. Anza[1], G. Bellettini[2], L. Bianchi[2,1], D. Bortoletto[3], M. Cremonesi[3], K. Knoepfel[4], Q. Liu[5], F. Margaroli[6], K. Potamianos[7], M. Trovato[2]

[1] *University of Pisa, Italy*

[2] *INFN Pisa, Italy*

[3] *Oxford University, UK*

[4] *FNAL, USA*

[5] *LANL, USA*

[6] *University of Rome "La Sapienza", Italy*

[7] *LBNL, USA*

Abstract

We present a search for W'-like resonances decaying to the tb final state. The search is performed in the $\not\!\!E_T$ plus jets sample using the full CDF dataset of 9.1 fb^{-1}. We select events with large missing transverse energy and two or three high-p_T jets, of which at least one is b-tagged. The reconstructed W' transverse invariant mass distribution is used to discriminate between signal and SM background. No significant excess above SM prediction is found. Using a benchmark $W' \to tb$ left-right symmetric model, we place 95% CL upper limits on the W' production cross section times branching ratio to tb. Assuming a W' with SM-like couplings and decay to leptons allowed (forbidden), we exclude $W' \to tb$ for W' masses below 820 (840) GeV/c^2. Relaxing the hypothesis on SM-like couplings, we exclude W' boson coupling strength values as a function of W' mass down to $g_{W'} = 0.4 g_{\rm SM}$ for $M_{W'} = 300$ GeV/c^2.

[1] ludobian@fnal.gov

1 Introduction

The existence of higher-mass W-like bosons, generically denoted as W', is predicted by several BSM models, including $SU(2)_R$ SM extensions [1], Kaluza-Klein extra-dimensions [2, 3], technicolor [4, 5] or Little Higgs scenarios [6]. Considering a simple reference left-right symmetric W' model, the main decay modes are the leptonic mode $W' \to \ell\nu$ and the hadronic mode $W' \to tb$. Searches for $W' \to tb$ extend the search for W' production to the more general cases of non-SM couplings with fermions, or where the leptonic decay is suppressed or forbidden.

The most recent searches for $W' \to tb$ have been carried out at the Tevatron collider by the CDF [7] and DØ [8] experiments, and at LHC by the ATLAS [9] and CMS [10] experiments. The plot on fig. 1 shows a comparison of the expected upper limits on $\sigma(p\bar{p} \to W') \times \mathcal{B}(W' \to tb)$ for the four most recent $W' \to tb$ searches. The limits are divided by the theoretical cross section in order to take into account the different W' production cross-section at Tevatron and LHC. By virtue of the higher c.m.s. energy available at LHC, the excluded mass range reach for a particular SM-like W' benchmark model is higher for ATLAS and CMS. However, because of the different ways in which production rates for quark-induced processes, such as W' production, and the dominant, gluon-induced SM backgrounds scale with greater c.m.s. energy [11], LHC experiments are less sensitive in the low W' mass region, where CDF has the most sensitive limits. Increasing the sensitivity in the low mass region allows to extend the search to exclude more general models with non-SM couplings, or generally lower $\sigma \times \mathcal{B}$. The goal of this analysis is thus to improve the CDF results using the full dataset in order to have the most sensitive limits on $\sigma(p\bar{p} \to W') \times \mathcal{B}(W' \to tb)$ in the low mass region.

Moreover, even though a simple reference W' model is used to model the signal, the analysis is valid for any massive state decaying to tb if its intrinsic width is less than the detector resolution. Results from this analysis can be used as a benchmark for searches for BSM processes with lower $\sigma \times \mathcal{B}$ (i.e., 2HDM charged Higgs $H^{\pm} \to tb$) and the same final state.

In this analysis, the search for $W' \to tb$ is performed in the $\not\!\!E_T$ plus jets channel. We employ data from the CDF high-$\not\!\!E_T$ triggers, selecting events compatible with the W plus two jets topology, in which the W decays to a neutrino and a high-p_T lepton (electron or muon), and the lepton is not

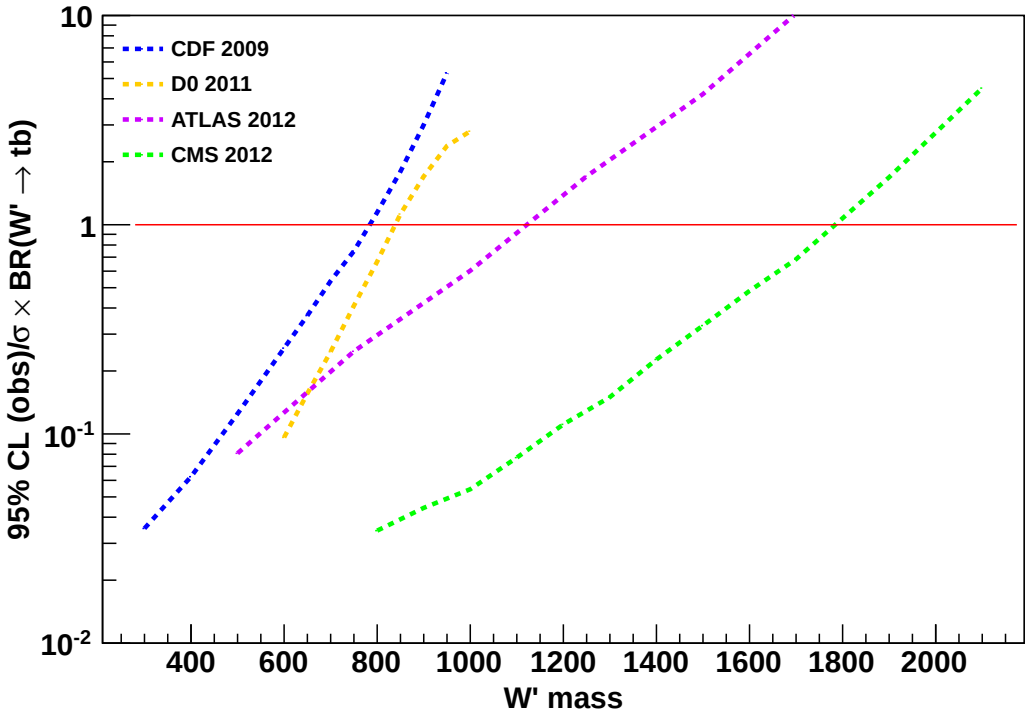

Figure 1 – Expected 95% CL upper limits on $\sigma(p\bar{p} \to W') \times \mathcal{B}(W' \to tb)$, divided by the theoretical value, for the most recent searches for $W' \to tb$ at hadron colliders. CDF has the most sensitive results in the low W' mass region $M_{W'} \leq 500$ GeV.

reconstructed. We include a third high-p_T jet to account for events in which the extra jet comes from initial or final state radiation (ISR/FSR), or from a hadronically decaying τ lepton originated from the W. Events in this sample are statistically independent from events in the lepton plus jets sample where a reconstructed electron or muon is required [12]. Results from this analysis can thus be combined with a future search in the leptons plus jets channel to obtain more stringent limits on $\sigma(p\bar{p} \to W') \times \mathcal{B}(W' \to tb)$.

2 Event selection

2.1 Online selection

For this analysis we use data from the high-$\not\!\!E_T$ data stream (emet) collected by CDF during the entirety of Run II, corresponding to an integrated luminosity of about 9.1 fb^{-1}. The online selection criteria, based on a logical OR combination of trigger paths MET_DIJET (p15-p38), MET_35_TWO_JETS (up to p4) and MET_35_CJET_JET (up to p14), require either $\not\!\!E_T^{\rm cal} > 45$ GeV, or $\not\!\!E_T^{\rm cal} > 35$ GeV and at least two jets.

2.2 Preselection cuts

A series of preselection cuts is applied to the resulting data sample. We exclude events containing identified electron or muon, and $\not\!\!E_T > 50$ GeV after corrections for instrumental effects in jet reconstruction [13]. The two jets of greatest E_T in the event are required to have transverse energies that satisfy $E_T^{j_1} > 25$ GeV and $E_T^{j_2} > 20$ GeV, respectively, according to a jet-energy determination based on calorimeter deposits and track momentum measurements [14]. Selected events are consistent with the W/Z + jets topology where the τ lepton in the $t \to Wb \to \tau\nu b$ channel is reconstructed as a jet in the calorimeter. To gain sensitivity in events with an unidentified τ lepton, we also accept events where the third-most energetic jet satisfies $E_T^{j_3} > 15$ GeV. We reject events with four reconstructed jets, where each jet exceeds the minimum transverse energy threshold ($E_T > 15$ GeV) and has pseudorapidity $|\eta| < 2.4$. To ensure that leading-E_T jets are within the silicon detector acceptance, they are required to satisfy $|\eta| < 2$, where at least one of them must satisfy $|\eta| < 0.9$.

One of the leading sources of significant $\not\!\!E_T$ in production of multijet events due to QCD arises from the mismeasurement of jet energies. Additionally, neutrinos from semileptonic b decays can also produce significant $\not\!\!E_T$ in these events. In both cases, the $\vec{\not\!\!E}_T$ is often aligned with $\vec{E}_{\rm T}^{j_2}$, and such events are rejected by requiring $\Delta\varphi(\vec{\not\!\!E}_T, \vec{E}_{\rm T}^{j_1}) \geq 1.5$ and $\Delta\varphi(\vec{\not\!\!E}_T, \vec{E}_{\rm T}^{j_{2,3}}) \geq 0.4$.

The large backgrounds from light-flavor jet production originating from u, d, or s quarks or gluons are reduced by identifying ("tagging") jets consistent with the decay of hadrons containing b quarks. For this analysis, the SecVTX (tight) and JetProb b-tagging algorithms are used. Events containing at least one of the leading jets tagged by SecVTX make up the tagged subsample. These events

are further subdivided into three mutually exclusive subsamples according to their tagging category, depending on whether they have exactly one SecVTX tagged jet (1T), one SecVTX and one JetProb tagged jet (TL) and two SecVTX tagged jets (TT).

3 Signal and background modeling

3.1 Signal

The most general Lagrangian describing the W' coupling to fermions can be written as

$$\mathcal{L} = \frac{g_{W'}}{\sqrt{2}} \bar{f}_i \gamma_\mu \left(a^L_{f_i f_j} P_L + a^R_{f_i f_j} P_R \right) W'^\mu f_j + \text{H.c.} \tag{1}$$

where $P_{L,R} = (1 \pm \gamma^5)/2$ are the projection operators, $g_{W'}$ is the gauge coupling, and the $a^{L,R}_{f_i f_j}$ are arbitrary couplings that may differ for quarks and leptons.

To generate MC simulations for signal events, we employ a simple reference W' model with purely left- or right-handed SM-like couplings to fermions, no interference with SM W, produced entirely via the s-channel diagram of fig. 2. The signal samples are generated by PYTHIA using the built-in W' definition (`masscode = 34`), with only the $W' \to tb$ decay channel open, in the mass range $200 \leq M_{W'} \leq 900$ GeV in 100 GeV intervals.

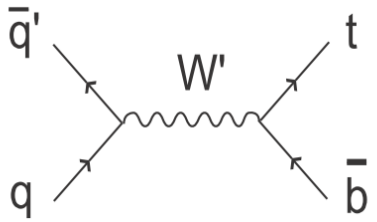

Figure 2 – Representative Feynman diagram for s-channel W' production and decay to tb.

From the point of view of our analysis, under these assumptions, a right-handed W'_R and a left-handed W'_L are equivalent. The only difference is in the branching ratio to tb, which will be different

$M_{W'}$ (GeV/c^2)	$\sigma \times \mathcal{B}$ (a) (pb)	$\sigma \times \mathcal{B}$ (b) (pb)	$\sigma \times \mathcal{B}$ (c) (pb)
200	39.43	57.39	-
300	44.14	61.46	1.59
400	16.65	22.65	1.17
500	5.922	7.953	0.84
600	2.100	2.790	0.44
700	0.743	0.974	0.32
800	0.262	0.337	0.26
900	0.093	0.116	0.26

Table 1 – Values for $\sigma(p\bar{p} \to W') \times \mathcal{B}(W' \to tb)$. From [15], theoretical NLO calculation (a) $W' \to \ell\nu$ allowed, (b) $W' \to \ell\nu$ forbidden. From [7], 95% CL observed limits.

for a W'_R depending whether the decay mode to leptons $W' \to \ell\nu$ is allowed or forbidden, as e.g. in the case where $M_{\nu_R} > M_{W'_R}$. Table 1 shows the theoretical prediction for $\sigma(p\bar{p} \to W') \times \mathcal{B}(W' \to tb)$ computed assuming a simple SM-like W' model in both cases where the leptonic decay mode is allowed or suppressed, along with observed limits from the most recent CDF analysis with 1.9 fb^{-1}.

3.2 Background processes

The main SM processes that contribute to the preselected sample are multijet production due to QCD (QCD multijet), W/Z + jets, top quark pair production $t\bar{t}$, electroweak single top production, and diboson.

Shape of distributions in top-quark events via pair and electroweak production, in W/Z + jets events, and in diboson events are modeled by MC simulation. The ALPGEN generator is used to simulate W/Z + jets; POWHEG is used for both $t\bar{t}$ and single top production; PYTHIA is used for diboson events. For each process, parton showering and hadronization is performed by PYTHIA. The event generation process includes a simulation of the detector response, and the resulting samples are subjected to the same reconstruction and analysis chain as the data. The normalization of templates for single top, diboson and $t\bar{t}$ is constrained to the respective theoretical cross section value.

A data-driven method based on a mistag matrix [16] is used to estimate the contribution to the tagged sample due to W/Z + jets and diboson processes with light flavor jets in the final state. W/Z + jets processes suffer from incorrectly predicted rates. For this reason, the normalization of W/Z + jets templates is left unconstrained in the final fit procedure. For prefit estimates we

employ the theoretical cross-section multiplied by a K-factor $K = 1.3$ to take into account NLO effects, with a 30% overall uncertainty.

A QCD multijet background model is derived from data events in a control region that consists almost entirely of QCD multijet contributions. A probability density function f_i is formed separately in each tagging category i ($i = \mathsf{1T}, \mathsf{TL}, \mathsf{TT}$) by taking the ratio between tagged and pretagged events as a function of several variables, as described in detail in [16]. A QCD multijet template is thus determined for each of the category i by weighting the untagged data in the preselection sample according to the f_i probability density functions. To determine the appropriate normalization for a given category, a scale factor is derived in a control region where the tagged diboson, top and W/Z + jets background estimates are subtracted from the tagged data, as described in appendix B.

To validate the background modeling, we compare tagged data and the corresponding combined background prediction for various kinematic, angular, and event-shape variables. Validation plots are presented in appendix C.

Process	Shape modeling	Cross Section (pb)
QCD multijet	data-driven	data-driven
W/Z + jets	ALPGEN + PYTHIA	data-driven
$t\bar{t}$	POWHEG	7.04 ± 0.44
single top (s-channel)	POWHEG	1.05 ± 0.17
single top (t-channel)	POWHEG	2.12 ± 0.32
WW	PYTHIA	12.4 ± 1.4
WZ	PYTHIA	3.7 ± 0.4
ZZ	PYTHIA	3.6 ± 0.4

Table 2 – Summary of methods for shape modeling and rate estimation.

4 QCDNN

QCD multijet events are the greatest contributor to the preselected sample, even after b-tag requirements. As a first background rejection step, we employ a multivariate method to separate QCD multijet background from the other background processes and the signal. For this purpose, a neural network QCDNN is trained to discriminate between QCD multijet and other processes. We then define the signal region with a minimum requirement of 0.45 on the resulting QCDNN distribution.

The application of this cut results in an increase of binned significance ranging from 30% to 200%, depending on the tagging category and the W' mass.

QCDNN is a feed-forward multilayer perceptron, as implemented in the TMVA package. A complete list of input variables is given in appendix A.

The training background sample consists of QCD multijet events, obtained from pretagged data as described in section 3.2. The training signal sample consists of single top s-channel events. Single top s-channel and $W' \to tb$ have the same final state topology, and similar kinematical distributions for those variable not related with the W' mass. This choice allows to perform the training exploiting the similarities between single top s-channel and $W' \to tb$ and the differences between the two processes and QCD multijet, while at the same time ensuring the same QCD multijet rejection performance for all W' mass points, since no bias due to information on $M_{W'}$ is introduced in the training process.

Figure 3 shows the QCDNN distribution in the preselection region.

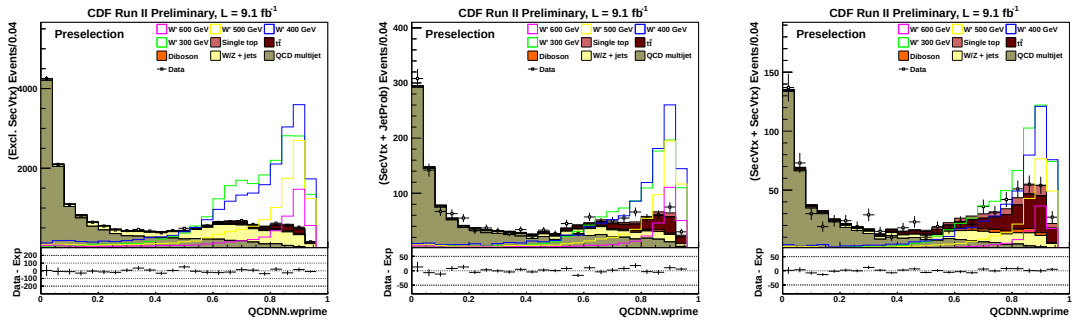

Figure 3 – QCDNN distribution in preselection region in the subsample with exactly one SecVTX tagged jet (left), one SecVTX and one JetProb tagged jet (middle) and two SecVTX tagged jets (right).

5 Final discriminant

As a final background discrimination step, a discriminating variable is chosen in order to have the maximum possible separation between the W' signal and the SM backgrounds. A tb pair originated from a W'-like state would appear as a resonant structure in the tb invariant mass spectrum; we choose $M_T(\not\!\!E_T, j_{1,2,3})$, the transverse invariant mass of the $\not\!\!E_T$ and the jets in the final state, corresponding to the W' transverse invariant mass. Since the final fit will be performed on this distribution, $M_T(\not\!\!E_T, j_{1,2,3})$ is the final discriminant for this analysis.

$W' \to tb$ in $\not\!\!E_T$+jets	CDF Run II Preliminary, L = 9.1 fb^{-1}		
	1T	TL	TT
QCD multijet	1871 ± 113	238 ± 26	71 ± 10
W/Z + jets	3757 ± 647	137 ± 25	94 ± 17
Diboson	239 ± 29	25 ± 3	24 ± 3
$t\bar{t}$	690 ± 73	142 ± 17	151 ± 18
Single top	272 ± 48	43 ± 8	51 ± 9
Total Background	6830 ± 663	584 ± 41	392 ± 28
Observed	6815	620	405
($M_{W'}$ = 300 GeV)	152 ± 47	54 ± 17	71 ± 22
($M_{W'}$ = 400 GeV)	150 ± 47	57 ± 18	60 ± 19
($M_{W'}$ = 500 GeV)	78 ± 25	32 ± 11	31 ± 10
($M_{W'}$ = 600 GeV)	35 ± 14	15 ± 6	12 ± 4

Table 3 – Expected and observed event yields in signal region defined by the QCDNN > 0.45 requirement in the subsample with exactly one SecVTX tagged jet (1T), one SecVTX and one JetProb tagged jet (TL) and two SecVTX tagged jets (TT). The uncertainties in the expected number of events are due to the uncertainties on the theoretical cross section and to the uncertainties on signal and background modeling. Signal estimates for four $M_{W'}$ hypotheses are also shown. Signal templates are normalized to observed limits from previous CDF analysis.

Figure 4 shows the $M_T(\not\!\!E_T, j_{1,2,3})$ distribution for events in the signal region.

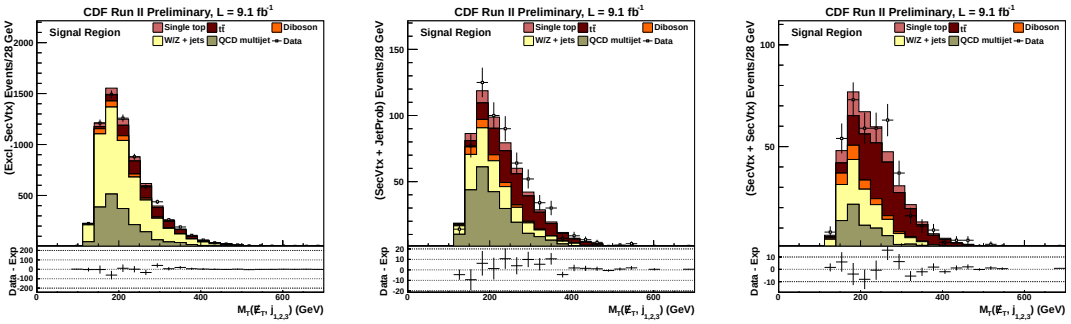

Figure 4 – $M_T(\not\!\!E_T, j_{1,2,3})$ distribution in signal region in the subsample with exactly one SecVTX tagged jet (left), one SecVTX and one JetProb tagged jet (middle) and two SecVTX tagged jets (right).

6 Systematic uncertainties

The systematic uncertainties considered in our analysis are grouped according to their sources, since the same source may affect the uncertainty of multiple background and signal distributions. Uncertainties due to the same source are considered 100% correlated. These uncertainties, which

apply to both signal and backgrounds, include luminosity measurement (6%), b-tagging efficiency (8 to 16%), trigger efficiency (1 to 3%), lepton veto efficiency (2%), parton distribution function (3%), and up to 6% for the jet-energy scale. Initial- and final-state radiation uncertainties (2%) are applied only to top processes ($t\bar{t}$ and single top).

The uncertainties due to simulations statistics, and the uncertainties on the normalization of $t\bar{t}$ (6%), single top (15%), diboson (6%) from the theoretical uncertainties, and QCD multijet (3 to 10%, calculated from scale factors) are not correlated.

Shapes obtained by varying the jet-energy scale by $\pm 1\sigma$ from its central values are associated to all MC-simulated processes as shape uncertainties. Shapes obtained by varying the f_i probability in each tagging category by $\pm 1\sigma$ are applied for the QCD multijet templates.

The W/Z + jets overall normalization is left unconstrained in the final fit. For W/Z + jets templates, the following additional uncertainties are considered:

- 30% uncertainty on the K-factor to correct the HF fraction for $W/Z + c\bar{c}$ and $W/Z + b\bar{b}$ events;
- 30% uncertainty to cover the extrapolation of the K-factor from the single-tag to the double-tag for $W/Z + c\bar{c}$ and $W/Z + b\bar{b}$ events;
- 30% uncertainty on the K-factor for $W + c$ events;
- 30% uncertainty on the K-factor for $W/Z +$ LF events ($W/Z +$ LF events with a jet matched to a heavy-flavor quark).

E_T-dependent uncertainty on b-tag scale factor

An additional uncertainty for of the b-tag efficiency scale factor (SF) is considered for signal templates. The b-jet originated from the W' bosons in $W' \to tb$ events have energies that can easily exceed those of the jets in the event sample used to measure the b-tag SF. We follow the approach already used in searches for massive resonances producing b quarks in the final state [17, 18]. First, we choose a parametrization for the extrapolation of the b-tag SF uncertainty outside the fiducial region. Then, we use these functions as per-event weights to create $\pm 1\sigma$ shifted templates for the b-tag uncertainty for each signal mass point. As the difference in shape among the original template and the shifted templates is negligible, only the resulting rate uncertainty is considered.

The parametrization we choose is the same used in Ref. [17], and it is the most conservative choice. According to this prescription, the b-tag SF uncertainty is symmetrical, and has a linear dependence on the jet E_T when the jet E_T is greater than 100 GeV. The corresponding weights for the $\pm 1\sigma$-shifted templates are thus

$$\pm 1\sigma = 1 \pm 0.0012(E_T(j_1) - 100 \text{ GeV}), \tag{2}$$

where $E_T(j_1)$ indicates the leading jet E_T. The effect of this uncertainty on the rate ranges from about 2% for low W' masses, to up to 30% for high W' masses.

As a consistency check, we apply the same procedure choosing the different jet E_T dependence used in Ref. [18]. The rate variation for signal templates thus obtained is consistent with results reported therein.

7 Limit calculation

Since the $M_T(\not\!\!E_T, j_{1,2,3})$ distribution shows no significant excess above SM predictions compatible with W'-like resonances, we calculate 95% CL upper limits on $\sigma(p\bar{p} \to W') \times \mathcal{B}(W' \to tb)$ by performing a binned maximum likelihood fit in the $M_T(\not\!\!E_T, j_{1,2,3})$ distribution, allowing for systematic and statistical fluctuations via template morphing. The procedure is implemented through the mclimit package. For each W' mass point we generate $N = 10000$ pseudoexperiments, with a systematic space sampling of $k = 1000000$.

The fit procedure is carried out simultaneously in the three independent subsamples 1S, SJ, SS. Figure 5 shows the results of the limit extraction for each tagging category separately, and for the three tagging categories combined. Most of our sensitivity is given by events in the two-tag subsamples SJ and SS, while events in the 1S subsample contribute significantly only for high $M_{W'}$ values.

Table 4 and figures 6–7 show the observed and expected limits obtained from our signal and background templates.

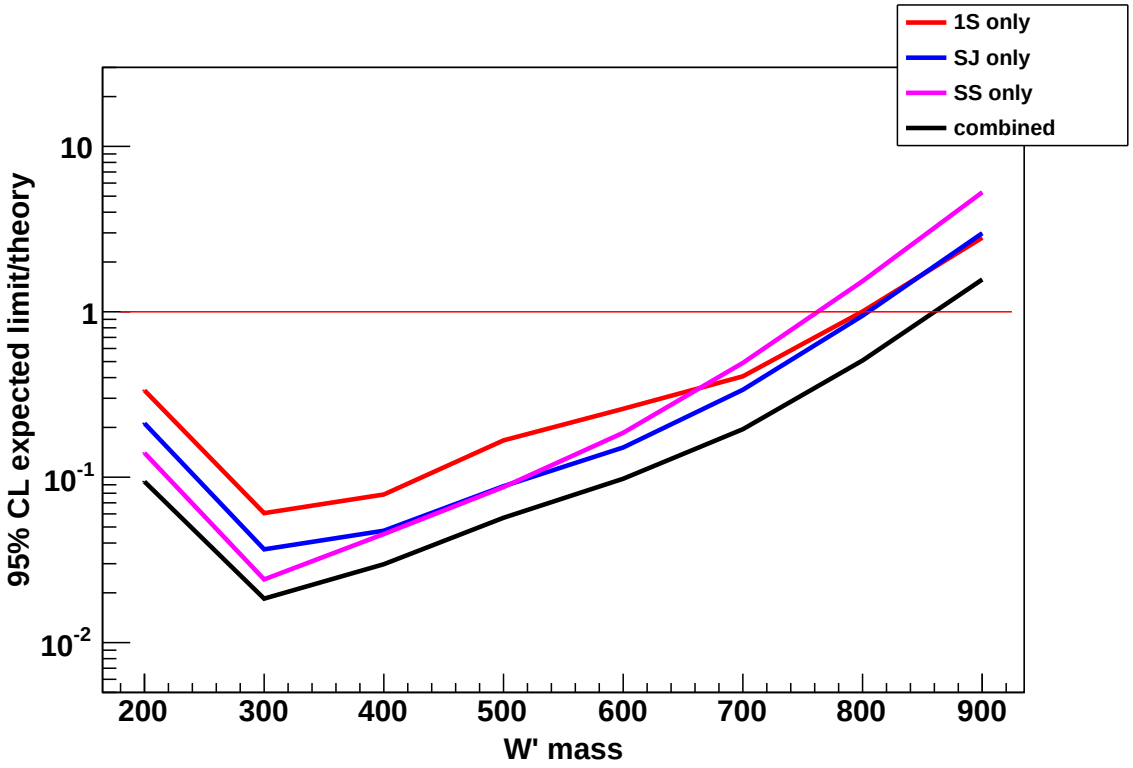

Figure 5 – 95% expected upper limits on $W' \to tb$ for each tagging category separately (color) and combined (black).

In fig. 6, the expected and observed limits on $\sigma(p\bar{p} \to W') \times \mathcal{B}(W' \to tb)$ are compared to the theoretical values computed for a simple reference W' model with SM-like couplings, in both cases where the leptonic decay $W' \to \ell\nu$ is allowed or forbidden. From the comparison of the line corresponding to the observed limits with the line corresponding to the theoretical prediction in the case where $W' \to \ell\nu$ is allowed (forbidden), we obtain an excluded mass range for values of $M_{W'} < 820$ GeV ($M_{W'} < 840$ GeV).

In fig. 7, the assumption of SM-like W' couplings is relaxed. A model with the same features as the reference W' with SM-like couplings g_{SM}, but for which $g_{W'} \neq g_{\mathrm{SM}}$, would differ from the reference model only for the overall normalization of $\sigma(p\bar{p} \to W') \times \mathcal{B}(W' \to tb)$. According to the tree-level diagram in fig. 2, the cross-section is proportional to g^4, so the ratio between the cross-section for the two models is equal to $g^4_{W'}/g^4_{\mathrm{SM}}$. For a given mass $M_{W'}$, $g_{W'}$ is adjusted until the normalized $\sigma(p\bar{p} \to W') \times \mathcal{B}(W' \to tb)$ equals the experimentally excluded value. This allows to define an

	95% C.L. limits on $\sigma(p\bar{p} \to W') \times \mathcal{B}(W' \to tb)$ [pb]	
$M_{W'}$ [GeV/c^2]	Expected $^{+1\sigma}_{-1\sigma}$	Observed
200	$5.40^{+3.30}_{-2.47}$	6.69
300	$1.13^{+0.60}_{-0.38}$	1.42
400	$0.70^{+0.33}_{-0.23}$	0.90
500	$0.49^{+0.25}_{-0.16}$	0.53
600	$0.31^{+0.14}_{-0.09}$	0.32
700	$0.22^{+0.10}_{-0.07}$	0.23
800	$0.21^{+0.10}_{-0.06}$	0.22
900	$0.21^{+0.10}_{-0.07}$	0.22

Table 4 – Observed and expected limits on $\sigma(p\bar{p} \to W') \times \mathcal{B}(W' \to tb)$. Theoretical predictions from [15] ($W' \to \ell\nu$ allowed).

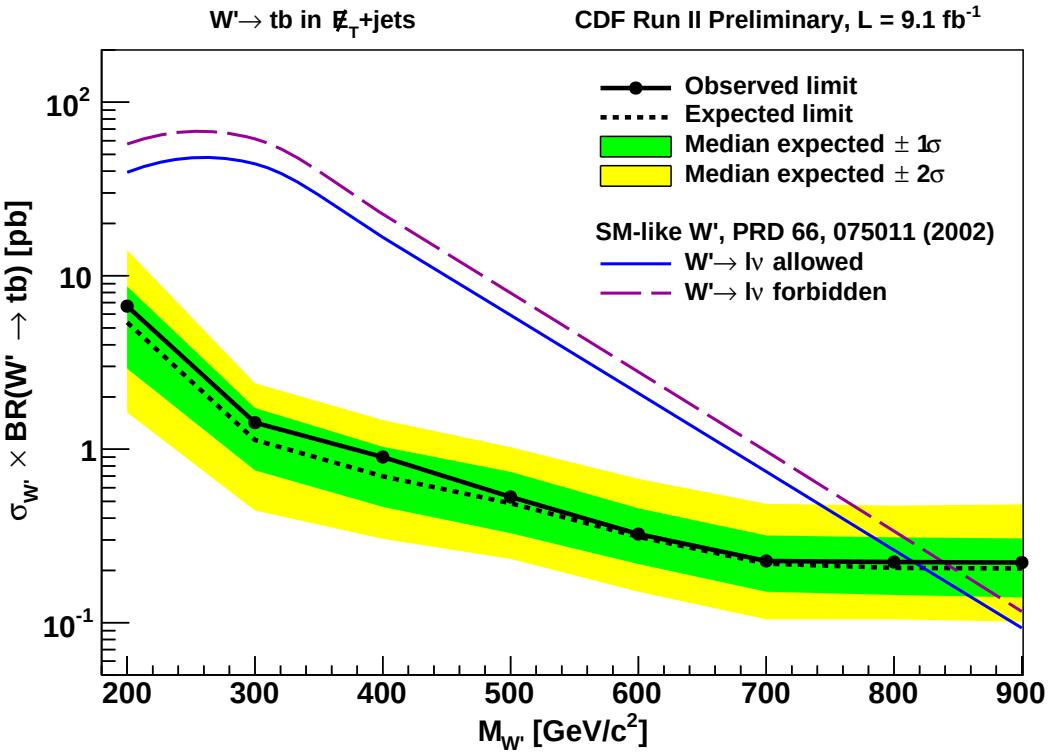

Figure 6 – Observed and expected limits on $\sigma(p\bar{p} \to W') \times \mathcal{B}(W' \to tb)$, with $\pm 1\sigma$ and $\pm 2\sigma$ confidence intervals. Theoretical predictions from [15].

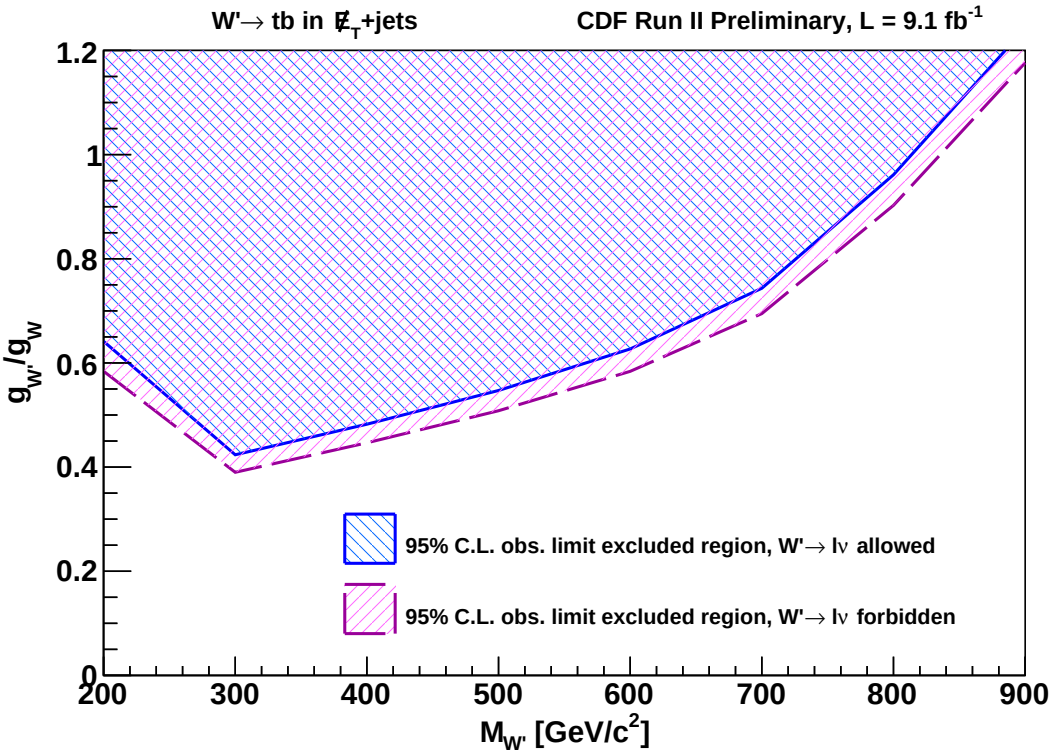

Figure 7 – Excluded regions in the $g_{W'}$-$M_{W'}$ plane, as obtained by observed limits and theoretical cross-section in both cases where the leptonic decay mode $W' \to \ell\nu$ is allowed or forbidden. Regions above each corresponding curve are excluded.

excluded region in the $M_{W'}$-$g_{W'}$ parameter space.

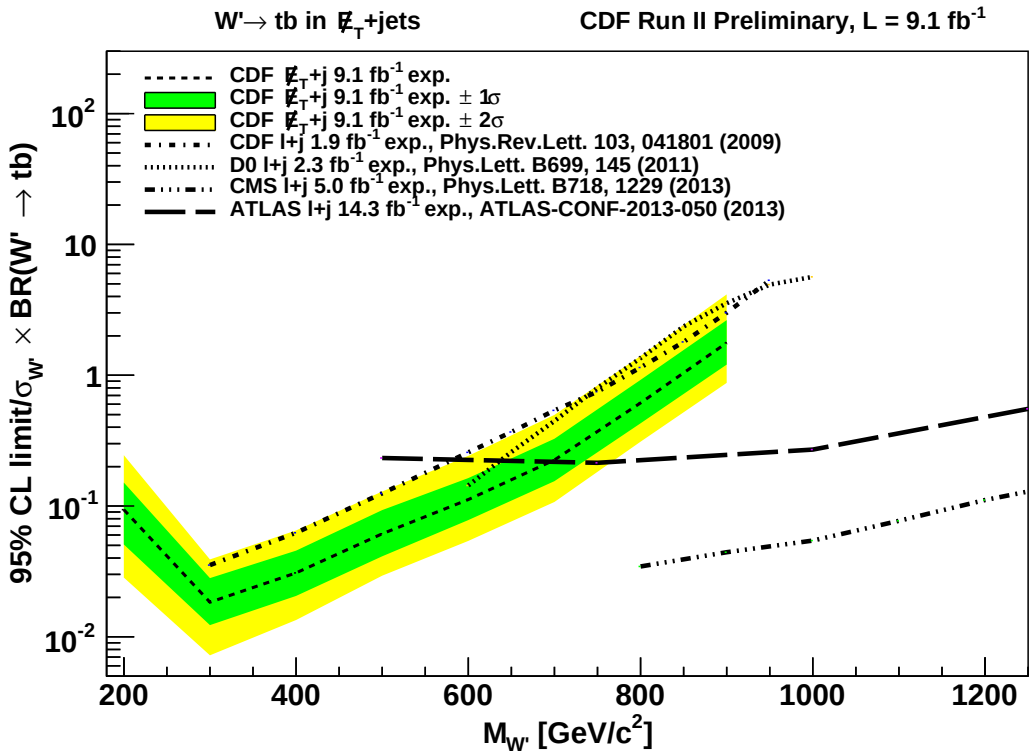

Figure 8 – Comparison among expected limits on $\sigma(p\bar{p} \to W') \times \mathcal{B}(W' \to tb)$ obtained with this analysis and the most recent results at other experiments. Limits from this analysis are the most sensitive in the W' mass region below 700 GeV.

8 Summary

In conclusion, we have presented a search for production of W'-like resonances decaying to tb in the $\not\!\!E_T$ plus jets final state, using the full CDF dataset of 9.1 fb^{-1}. We have compared observed data and SM background predictions in the transverse invariant mass of the $\not\!\!E_T$ and jets distribution. No significant evidence for resonant tb production is found. We place upper limits on $\sigma(p\bar{p} \to W') \times \mathcal{B}(W' \to tb)$ using a simple left-right symmetric W' reference model. Assuming that the decay $W' \to \ell\nu$ is allowed (not allowed), we exclude at the 95% CL a W' with SM-like couplings for masses below 820 GeV (840 GeV). Relaxing the assumptions on SM-like couplings, we exclude $g_{W'}$ up to values of $g_{W'} > 0.4 g_{\rm SM}$ for $M_{W'} = 300$ GeV. Limits from this analysis are currently the most sensitive in the region $M_{W'} < 600$ GeV.

References

[1] Jogesh C. Pati and Abdus Salam. Lepton Number as the Fourth Color. *Phys.Rev.*, D10:275–289, 1974.

[2] Yukihiro Mimura and S. Nandi. Orbifold breaking of left-right gauge symmetry. *Phys.Lett.*, B538:406–414, 2002.

[3] Gustavo Burdman, Bogdan A. Dobrescu, and Eduardo Ponton. Resonances from two universal extra dimensions. *Phys.Rev.*, D74:075008, 2006.

[4] Howard Georgi, Elizabeth Ellen Jenkins, and Elizabeth H. Simmons. The Ununified Standard Model. *Nucl.Phys.*, B331:541, 1990.

[5] Ehab Malkawi, Timothy M.P. Tait, and C.P. Yuan. A Model of strong flavor dynamics for the top quark. *Phys.Lett.*, B385:304–310, 1996.

[6] Maxim Perelstein. Little Higgs models and their phenomenology. *Prog.Part.Nucl.Phys.*, 58:247–291, 2007.

[7] T. Aaltonen et al. Search for the Production of Narrow t anti-b Resonances in 1.9 fb-1 of $p\bar{p}$ Collisions at $\sqrt{s} = 1.96$ TeV. *Phys.Rev.Lett.*, 103:041801, 2009.

[8] Victor Mukhamedovich Abazov et al. Search for $W' \to tb$ resonances with left- and right-handed couplings to fermions. *Phys.Lett.*, B699:145–150, 2011.

[9] Georges Aad et al. Search for tb resonances in proton-proton collisions at $\sqrt{s} = 7$ TeV with the ATLAS detector. *Phys.Rev.Lett.*, 109:081801, 2012.

[10] Serguei Chatrchyan et al. Search for a W ' boson decaying to a bottom quark and a top quark in pp collisions at $\sqrt{s} = 7$ TeV. *Phys.Lett.*, B718:1229–1251, 2013.

[11] Daniel Duffty and Zack Sullivan. Model independent reach for W-prime bosons at the LHC. *Phys.Rev.*, D86:075018, 2012.

[12] A. Apresyan et al. Event selection for higgs search in the $\not\!\!E_T$ plus jets sample.

[13] A. Bhatti et al. Determination of the jet energy scale at the collider detector at Fermilab. *Nucl.Instrum.Meth.*, A566:375–412, 2006.

[14] C. Adloff et al. Diffraction dissociation in photoproduction at HERA. *Z.Phys.*, C74:221–236, 1997.

[15] Zack Sullivan. Fully differential W' production and decay at next-to-leading order in qcd. *Phys. Rev. D*, 66:075011, Oct 2002.

[16] F. Margaroli D. Bortoletto Q. Liu, K. Potamianos. Background estimation in met + b-jets analysis.

[17] J. Vizan F. Sforza C. Group, Y. Oksuzian. Search for the resonant $t\bar{t}$ production with full tevatron dataset $\int \mathcal{L}dt = 9.45$ fb^{-1}.

[18] Catalin Ciobanu Peter Dong Bernd Stelzer Rainer Wallny Dan Amidei, J. Clark Cully. W'-like resonances in the tb decay channel with 1.9 fb-1.

A QCDNN input variables

In the following, the complete list of the 13 QCDNN input variables is given.

- Missing transverse momentum, $\not{p}_T$
- Missing transverse energy, $\not{E}_T$
- Difference in ϕ between missing transverse energy $\not{E}_T$ and missing transverse momentum $\not{p}_T$, $\Delta\phi(\not{E}_T, \not{p}_T)$
- Maximum difference in R-space between two jets, for all jet pairs
- Minimum difference in ϕ between the $\not{E}_T$ and each jet
- Minimum difference in ϕ between the $\not{p}_T$ and the jets, considering all $(\not{p}_T, j_i)$ pairings
- Maximum difference in ϕ between jet directions, for all jet pairs;
- Ratio of H_T, vector sum of *tight* jet E_T, over $\not{E}_T$
- $\Delta\phi$ between the direction of the leading jets in the jet pair rest frame and the direction of the jet pair boost
- metsig, the ratio between $\not{E}_T$ and the square root of the summed E_T over all calorimetric activity
- Event sphericity $S = 1.5 \times (\lambda_2 + \lambda_3)$, where the λ_i are the eigenvalues of the sphericity tensor[2].
- Invariant mass of $\not{E}_T$, j_1 and j_2

[2]For N particles, if p_i is the momentum of the ith particle, the sphericity tensor is defined as $M_{\alpha\beta} = \sum_{i=1}^{N} p_{i\alpha} p_{i\beta}$, $(\alpha, \beta = x, y, z)$.

B QCD multijet normalization

We derive the QCD multijet normalization as a scale factor k_{QCD} to be applied to the tag rate prediction in the $0 \leq \mathsf{QCDNN} < 0.1$ region A:

$$k_{\mathrm{QCD}} = \frac{N_A(\mathrm{data}) - \sum_i N_A^i(\mathrm{MC}_i)}{N_A(\mathrm{QCD})},$$

where $i = t\bar{t}$, W/Z + jets, diboson, single top.

We take the uncertainty on k_{QCD} as a systematic uncertainty on QCD normalization:

$$\frac{\delta k_{\mathrm{QCD}}}{k_{\mathrm{QCD}}} = \sqrt{\left(\sum_i \frac{\sqrt{\delta \mathrm{MC}_i^2(\mathrm{stat}) + \delta \mathrm{MC}_i^2(\mathrm{syst})}}{\mathrm{data} - \mathrm{MC}_i}\right)^2 + \left(\frac{\delta N_A(\mathrm{QCD})}{N_A(\mathrm{QCD})}\right)^2},$$

Since W/Z + jets is going to be unconstrained in the final fit, at this level we give a 100% uncertainty to its normalization to estimate the δk_{QCD}.

C Validation plots in signal region

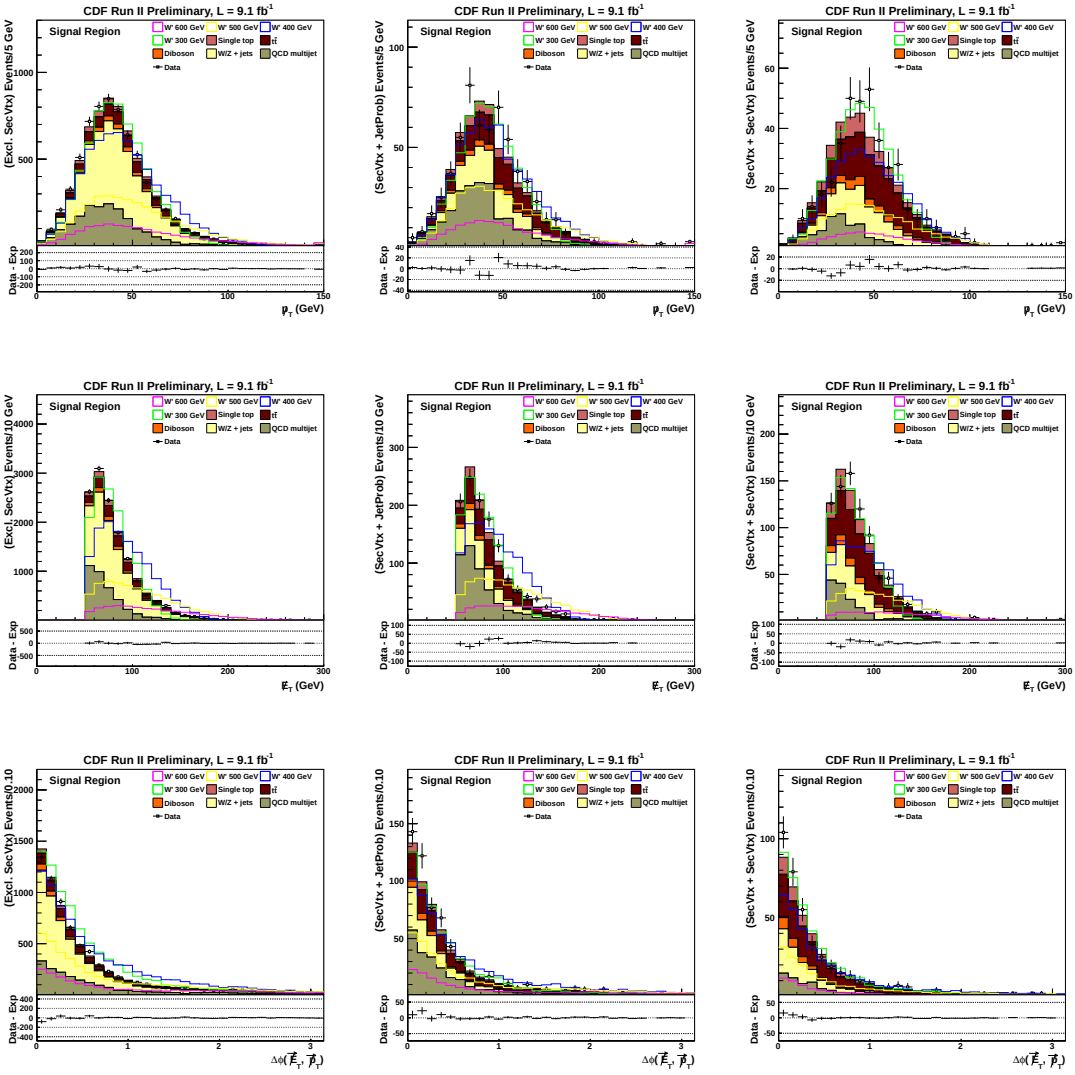

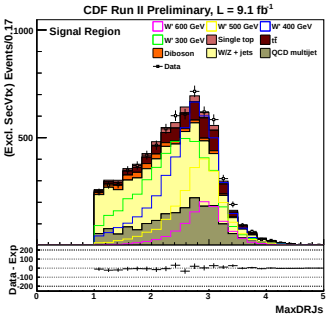
CDF Run II Preliminary, L = 9.1 fb-1
Signal Region
W' 600 GeV
W' 500 GeV
W' 400 GeV
W' 300 GeV
Single top
tt̄
Diboson
W/Z + jets
QCD multijet
Data
(Excl. SecVtx) Events/0.17
Data - Exp
MaxDRJs

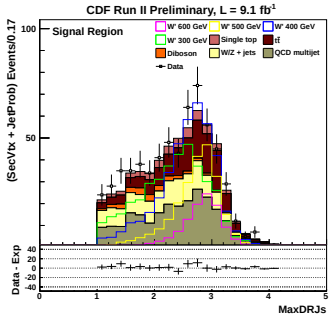
CDF Run II Preliminary, L = 9.1 fb-1
Signal Region
W' 600 GeV
W' 500 GeV
W' 400 GeV
W' 300 GeV
Single top
tt̄
Diboson
W/Z + jets
QCD multijet
Data
(SecVtx + JetProb) Events/0.17
Data - Exp
MaxDRJs

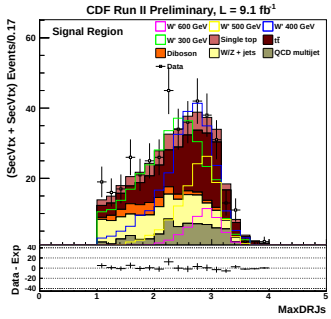
CDF Run II Preliminary, L = 9.1 fb-1
Signal Region
W' 600 GeV
W' 500 GeV
W' 400 GeV
W' 300 GeV
Single top
tt̄
Diboson
W/Z + jets
QCD multijet
Data
(SecVtx + SecVtx) Events/0.17
Data - Exp
MaxDRJs

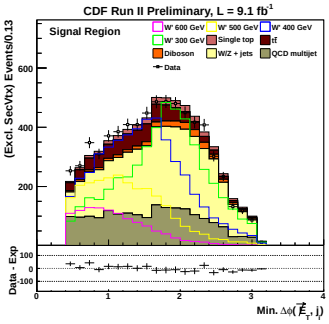
CDF Run II Preliminary, L = 9.1 fb-1
Signal Region
W' 600 GeV
W' 500 GeV
W' 400 GeV
W' 300 GeV
Single top
tt̄
Diboson
W/Z + jets
QCD multijet
Data
(Excl. SecVtx) Events/0.13
Data - Exp
Min. Δφ(Ê_T, j_i)

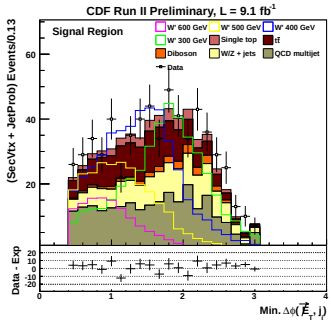
CDF Run II Preliminary, L = 9.1 fb-1
Signal Region
W' 600 GeV
W' 500 GeV
W' 400 GeV
W' 300 GeV
Single top
tt̄
Diboson
W/Z + jets
QCD multijet
Data
(SecVtx + JetProb) Events/0.13
Data - Exp
Min. Δφ(Ê_T, j_i)

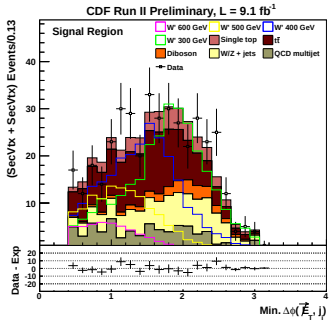
CDF Run II Preliminary, L = 9.1 fb-1
Signal Region
W' 600 GeV
W' 500 GeV
W' 400 GeV
W' 300 GeV
Single top
tt̄
Diboson
W/Z + jets
QCD multijet
Data
(SecVtx + SecVtx) Events/0.13
Data - Exp
Min. Δφ(Ê_T, j_i)

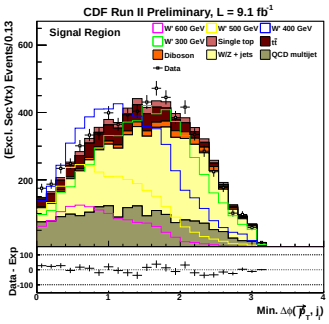
CDF Run II Preliminary, L = 9.1 fb-1
Signal Region
W' 600 GeV
W' 500 GeV
W' 400 GeV
W' 300 GeV
Single top
tt̄
Diboson
W/Z + jets
QCD multijet
Data
(Excl. SecVtx) Events/0.13
Data - Exp
Min. Δφ(p⃗_T, j_i)

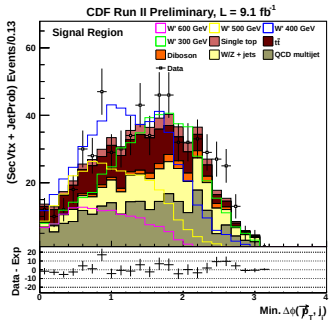
CDF Run II Preliminary, L = 9.1 fb-1
Signal Region
W' 600 GeV
W' 500 GeV
W' 400 GeV
W' 300 GeV
Single top
tt̄
Diboson
W/Z + jets
QCD multijet
Data
(SecVtx + JetProb) Events/0.13
Data - Exp
Min. Δφ(p⃗_T, j_i)

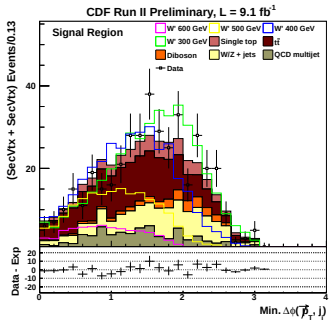
CDF Run II Preliminary, L = 9.1 fb-1
Signal Region
W' 600 GeV
W' 500 GeV
W' 400 GeV
W' 300 GeV
Single top
tt̄
Diboson
W/Z + jets
QCD multijet
Data
(SecVtx + SecVtx) Events/0.13
Data - Exp
Min. Δφ(p⃗_T, j_i)

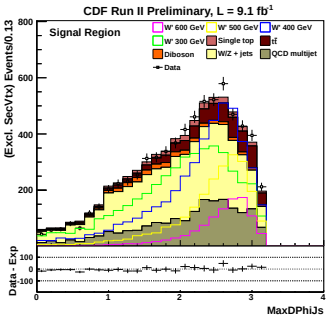
CDF Run II Preliminary, L = 9.1 fb-1
Signal Region
W' 600 GeV
W' 500 GeV
W' 400 GeV
W' 300 GeV
Single top
tt̄
Diboson
W/Z + jets
QCD multijet
Data
(Excl. SecVtx) Events/0.13
Data - Exp
MaxDPhiJs

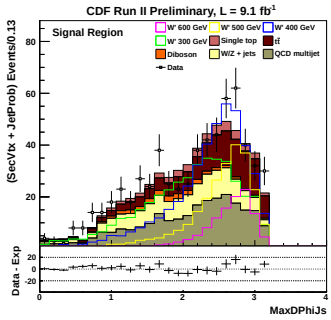
CDF Run II Preliminary, L = 9.1 fb-1
Signal Region
W' 600 GeV
W' 500 GeV
W' 400 GeV
W' 300 GeV
Single top
tt̄
Diboson
W/Z + jets
QCD multijet
Data
(SecVtx + JetProb) Events/0.13
Data - Exp
MaxDPhiJs

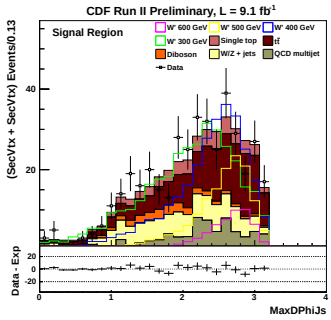
CDF Run II Preliminary, L = 9.1 fb-1
Signal Region
W' 600 GeV
W' 500 GeV
W' 400 GeV
W' 300 GeV
Single top
tt̄
Diboson
W/Z + jets
QCD multijet
Data
(SecVtx + SecVtx) Events/0.13
Data - Exp
MaxDPhiJs

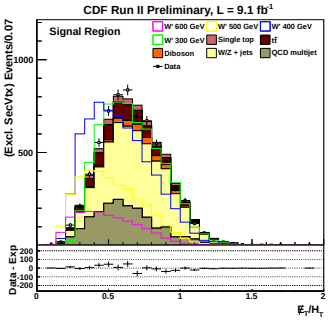
CDF Run II Preliminary, L = 9.1 fb-1
Signal Region
W' 600 GeV
W' 500 GeV
W' 400 GeV
W' 300 GeV
Single top
tt̄
Diboson
W/Z + jets
QCD multijet
Data
(Excl. SecVtx) Events/0.07
Data - Exp
E̸T/HT

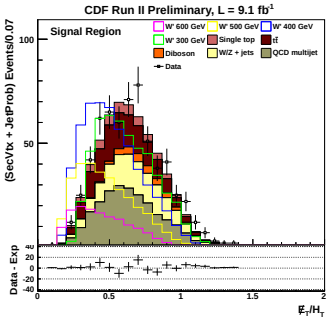
CDF Run II Preliminary, L = 9.1 fb-1
Signal Region
W' 600 GeV
W' 500 GeV
W' 400 GeV
W' 300 GeV
Single top
tt̄
Diboson
W/Z + jets
QCD multijet
Data
(SecVtx + JetProb) Events/0.07
Data - Exp
E̸T/HT

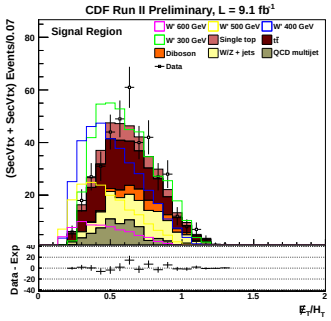
CDF Run II Preliminary, L = 9.1 fb-1
Signal Region
W' 600 GeV
W' 500 GeV
W' 400 GeV
W' 300 GeV
Single top
tt̄
Diboson
W/Z + jets
QCD multijet
Data
(SecVtx + SecVtx) Events/0.07
Data - Exp
E̸T/HT

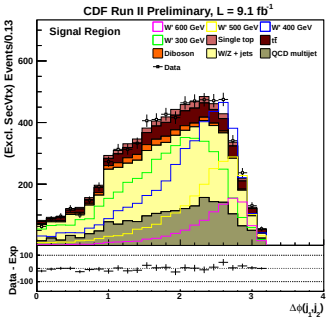
CDF Run II Preliminary, L = 9.1 fb-1
Signal Region
W' 600 GeV
W' 500 GeV
W' 400 GeV
W' 300 GeV
Single top
tt̄
Diboson
W/Z + jets
QCD multijet
Data
(Excl. SecVtx) Events/0.13
Data - Exp
Δφ(j1,j2)

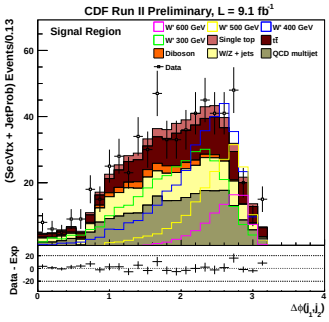
CDF Run II Preliminary, L = 9.1 fb-1
Signal Region
W' 600 GeV
W' 500 GeV
W' 400 GeV
W' 300 GeV
Single top
tt̄
Diboson
W/Z + jets
QCD multijet
Data
(SecVtx + JetProb) Events/0.13
Data - Exp
Δφ(j1,j2)

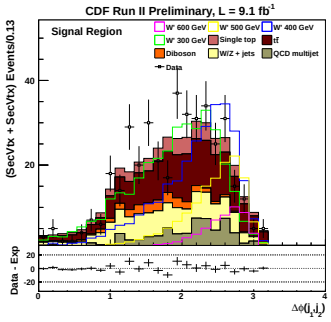
CDF Run II Preliminary, L = 9.1 fb-1
Signal Region
W' 600 GeV
W' 500 GeV
W' 400 GeV
W' 300 GeV
Single top
tt̄
Diboson
W/Z + jets
QCD multijet
Data
(SecVtx + SecVtx) Events/0.13
Data - Exp
Δφ(j1,j2)

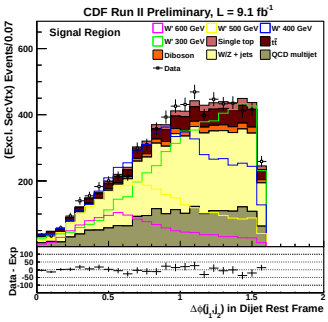
CDF Run II Preliminary, L = 9.1 fb-1
Signal Region
W' 600 GeV
W' 500 GeV
W' 400 GeV
W' 300 GeV
Single top
tt̄
Diboson
W/Z + jets
QCD multijet
Data
(Excl. SecVtx) Events/0.07
Data - Exp
Δφ(j1,j2) in Dijet Rest Frame

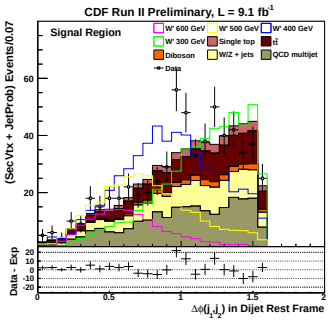
CDF Run II Preliminary, L = 9.1 fb-1
Signal Region
W' 600 GeV
W' 500 GeV
W' 400 GeV
W' 300 GeV
Single top
tt̄
Diboson
W/Z + jets
QCD multijet
Data
(SecVtx + JetProb) Events/0.07
Data - Exp
Δφ(j1,j2) in Dijet Rest Frame

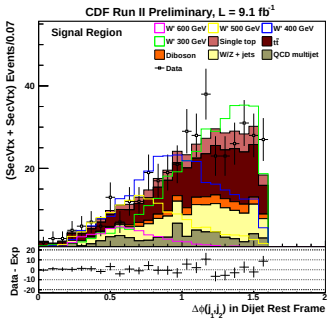
CDF Run II Preliminary, L = 9.1 fb-1
Signal Region
W' 600 GeV
W' 500 GeV
W' 400 GeV
W' 300 GeV
Single top
tt̄
Diboson
W/Z + jets
QCD multijet
Data
(SecVtx + SecVtx) Events/0.07
Data - Exp
Δφ(j1,j2) in Dijet Rest Frame

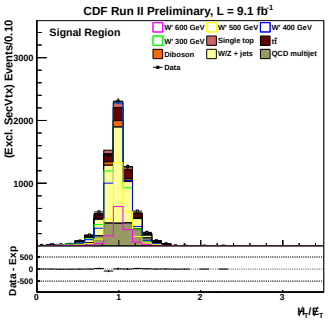
CDF Run II Preliminary, L = 9.1 fb-1
Signal Region
W' 600 GeV
W' 500 GeV
W' 400 GeV
W' 300 GeV
Single top
tt̄
Diboson
W/Z + jets
QCD multijet
Data
(Excl. SecVtx) Events/0.10
Data - Exp
H̸T/E̸T

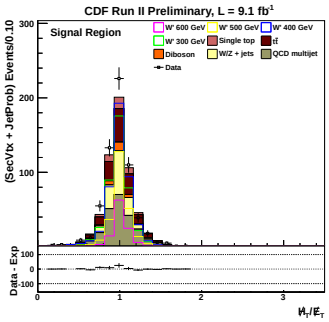
CDF Run II Preliminary, L = 9.1 fb-1
Signal Region
W' 600 GeV
W' 500 GeV
W' 400 GeV
W' 300 GeV
Single top
tt̄
Diboson
W/Z + jets
QCD multijet
Data
(SecVtx + JetProb) Events/0.10
Data - Exp
H̸T/E̸T

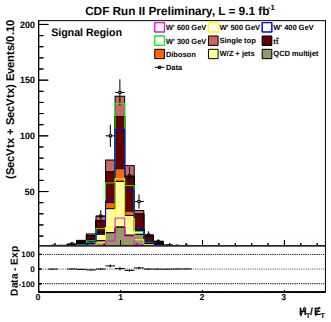
CDF Run II Preliminary, L = 9.1 fb-1
Signal Region
W' 600 GeV
W' 500 GeV
W' 400 GeV
W' 300 GeV
Single top
tt̄
Diboson
W/Z + jets
QCD multijet
Data
(SecVtx + SecVtx) Events/0.10
Data - Exp
H̸T/E̸T

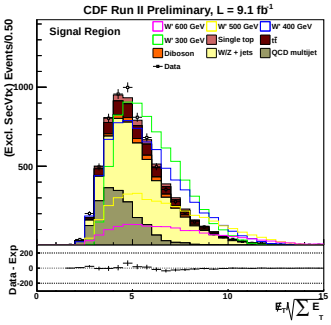
CDF Run II Preliminary, L = 9.1 fb-1
Signal Region
W' 600 GeV
W' 500 GeV
W' 400 GeV
W' 300 GeV
Single top
tt̄
Diboson
W/Z + jets
QCD multijet
Data
(Excl. SecVtx) Events/0.50
Data - Exp
E_T/√(Σ E_T)

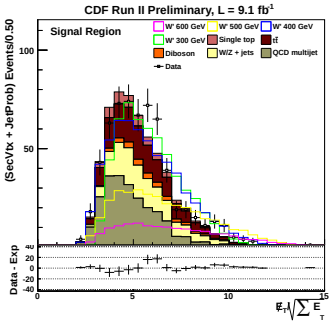
CDF Run II Preliminary, L = 9.1 fb-1
Signal Region
W' 600 GeV
W' 500 GeV
W' 400 GeV
W' 300 GeV
Single top
tt̄
Diboson
W/Z + jets
QCD multijet
Data
(SecVtx + JetProb) Events/0.50
Data - Exp
E_T/√(Σ E_T)

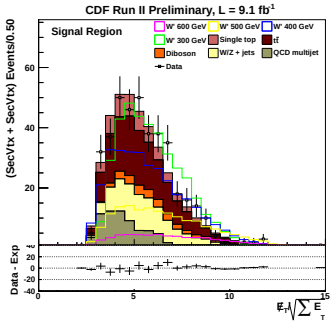
CDF Run II Preliminary, L = 9.1 fb-1
Signal Region
W' 600 GeV
W' 500 GeV
W' 400 GeV
W' 300 GeV
Single top
tt̄
Diboson
W/Z + jets
QCD multijet
Data
(SecVtx + SecVtx) Events/0.50
Data - Exp
E_T/√(Σ E_T)

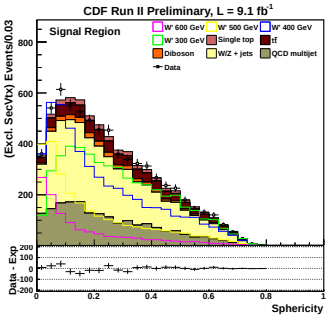
CDF Run II Preliminary, L = 9.1 fb-1
Signal Region
W' 600 GeV
W' 500 GeV
W' 400 GeV
W' 300 GeV
Single top
tt̄
Diboson
W/Z + jets
QCD multijet
Data
(Excl. SecVtx) Events/0.03
Data - Exp
Sphericity

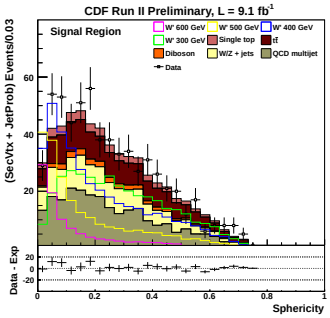
CDF Run II Preliminary, L = 9.1 fb-1
Signal Region
W' 600 GeV
W' 500 GeV
W' 400 GeV
W' 300 GeV
Single top
tt̄
Diboson
W/Z + jets
QCD multijet
Data
(SecVtx + JetProb) Events/0.03
Data - Exp
Sphericity

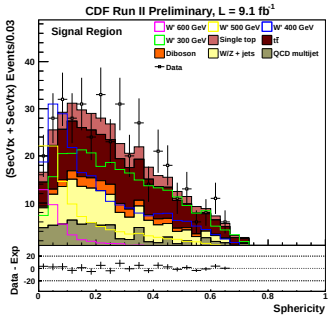
CDF Run II Preliminary, L = 9.1 fb-1
Signal Region
W' 600 GeV
W' 500 GeV
W' 400 GeV
W' 300 GeV
Single top
tt̄
Diboson
W/Z + jets
QCD multijet
Data
(SecVtx + SecVtx) Events/0.03
Data - Exp
Sphericity

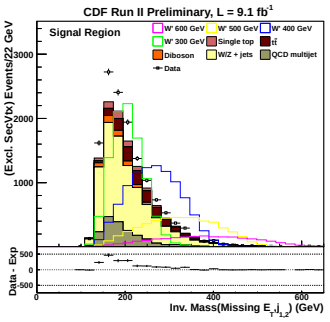
CDF Run II Preliminary, L = 9.1 fb-1
Signal Region
W' 600 GeV
W' 500 GeV
W' 400 GeV
W' 300 GeV
Single top
tt̄
Diboson
W/Z + jets
QCD multijet
Data
(Excl. SecVtx) Events/22 GeV
Data - Exp
Inv. Mass(Missing E_T,j1,j2) (GeV)

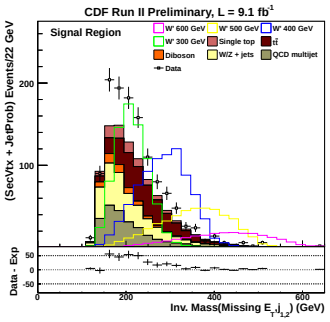
CDF Run II Preliminary, L = 9.1 fb-1
Signal Region
W' 600 GeV
W' 500 GeV
W' 400 GeV
W' 300 GeV
Single top
tt̄
Diboson
W/Z + jets
QCD multijet
Data
(SecVtx + JetProb) Events/22 GeV
Data - Exp
Inv. Mass(Missing E_T,j1,j2) (GeV)

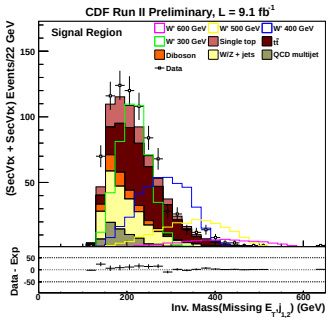
CDF Run II Preliminary, L = 9.1 fb-1
Signal Region
W' 600 GeV
W' 500 GeV
W' 400 GeV
W' 300 GeV
Single top
tt̄
Diboson
W/Z + jets
QCD multijet
Data
(SecVtx + SecVtx) Events/22 GeV
Data - Exp
Inv. Mass(Missing E_T,j1,j2) (GeV)

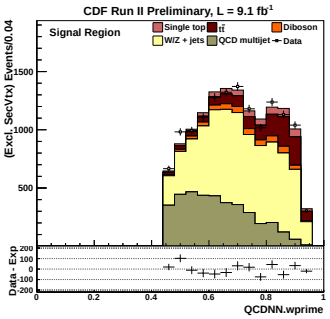
CDF Run II Preliminary, L = 9.1 fb-1
Signal Region
Single top
tt̄
Diboson
W/Z + jets
QCD multijet
Data
(Excl. SecVtx) Events/0.04
Data - Exp
QCDNN.wprime

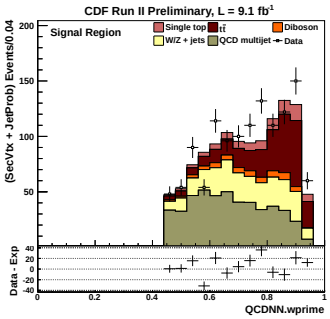
CDF Run II Preliminary, L = 9.1 fb-1
Signal Region
Single top
tt̄
Diboson
W/Z + jets
QCD multijet
Data
(SecVtx + JetProb) Events/0.04
Data - Exp
QCDNN.wprime

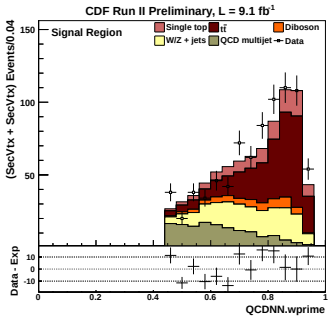
CDF Run II Preliminary, L = 9.1 fb-1
Signal Region
Single top
tt̄
Diboson
W/Z + jets
QCD multijet
Data
(SecVtx + SecVtx) Events/0.04
Data - Exp
QCDNN.wprime